Comparative genomics reveals intra and inter species variation in the pathogenic fungus *Batrachochytrium dendrobatidis*

Mark N. Yacoub[a] and Jason E. Stajich[a,b]

[a]Department of Microbiology and Plant Pathology, University of California Riverside, Riverside, California 92521 USA
[b]Institute for Integrative Genome Biology, University of California Riverside, Riverside, California 92521, USA

[*]Address correspondence to:

Mark N. Yacoub, mark.yacoub@ucr.edu

Jason E. Stajich, jason.stajich@ucr.edu

Abstract

The Global Pandemic Lineage (GPL) of the amphibian pathogen *Batrachochytrium dendrobatidis* (*Bd*) has been described as a main driver of amphibian extinctions on nearly every continent. Near complete genome of three *Bd*-GPL strains have enabled studies of the pathogen but the genomic features that set *Bd*-GPL apart from other *Bd* lineages is not well understood due to a lack of high-quality genome assemblies and annotations from other lineages. We used long-read DNA sequencing to assemble high-quality genomes of three *Bd*-BRAZIL isolates and one non-pathogen outgroup species *Polyrhizophydium stewartii* (*Ps*) strain JEL0888, and compared these to genomes of previously sequenced *Bd*-GPL strains. The *Bd*-BRAZIL assemblies range in size between 22.0 and 26.1 Mb and encode 8495-8620 protein-coding genes for each strain. Our pan-genome analysis provided insight into shared and lineage-specific gene

content. The core genome of *Bd* consists of 6278 conserved gene families, with 202 *Bd*-BRAZIL and 172 *Bd*-GPL specific gene families. We discovered gene copy number variation in pathogenicity gene families between *Bd*-BRAZIL and *Bd*-GPL strains though none were consistently expanded in *Bd*-GPL or *Bd*-BRAZIL strains. Comparison within the Batrachochytrium genus and two closely related non-pathogenic saprophytic chytrids identified variation in sequence and protein domain counts. We further test these new Bd-BRAZIL genomes to assess their utility as reference genomes for transcriptome alignment and analysis. Our analysis examines the genomic variation between strains in *Bd*-BRAZIL and *Bd*-GPL and offers insights into the application of these genomes as reference genomes for future studies.

Key Words: Pangenome, *Batrachochytrium dendrobatidis,* genome diversity, pathogenicity genes, comparative genomics

Introduction

Batrachochytrium dendrobatidis (*Bd*) is a chytrid fungus and causative agent of the disease chytridiomycosis (Kilpatrick et al. 2010; Daszak et al. 1999; Longcore et al. 1999). The disease is widespread among amphibian populations and has contributed to declines on five continents (Scheele et al. 2019). The pathogen is globally distributed and genetically diverse, with strains being represented in described lineages; *Bd*-CAPE, *Bd*-ASIA-2/BRAZIL (hereafter *Bd*-BRAZIL), *Bd*-ASIA, and *Bd*-GPL (Global Panzootic Lineage) (Farrer et al. 2011; Schloegel et al. 2012; Rosenblum et al. 2013; Farrer et al.

2013; O'Hanlon et al. 2018; Byrne et al. 2019). Among these lineages, the *Bd*-GPL lineage alone is implicated in the majority of amphibian declines (Belasen et al. 2022; Becker et al. 2017; Farrer et al. 2011). The emergence of the *Bd*-GPL lineage has been suggested to be a more recent expansion, occurring in the late 20th century (O'Hanlon et al. 2018).The other three lineages are genetically divergent from the *Bd*-GPL strains but are less widespread (Belasen et al. 2022). The genetic diversity between the other *Bd* lineages and the recent evolution of *Bd*-GPL suggests the possibility of gene expansions in *Bd*-GPL strains related to pathogenicity(Joneson et al. 2011; Farrer et al. 2017).

Despite the pathogen's importance, little is known about the gene content variation between *Bd* strains. The majority of genetic and genomic studies have relied on the reference genomes of two *Bd*-GPL strains, JEL423 and JAM81 (Joneson et al. 2011; Farrer et al. 2017). No contiguous genomes of *Bd* strains from any other lineage have been provided until now. Among the enzootic *Bd* lineages, *Bd-BRAZIL* has been previously compared with the *Bd*-GPL through comparative transcriptomics, regional distribution and virulence analysis (Becker et al. 2017; McDonald et al. 2020). Although strains from both lineages co-occur in South America, the *Bd*-GPL strains have been observed to be geographically unstructured and more infective towards amphibians in the Brazilian Atlantic Forest (Jenkinson et al. 2016; Greenspan et al. 2018).

Close relatives of *Bd* (e.g., *Homolaphlyctis polyrhiza* [*Hp*]) are saprophytic while the genus *Batrachochytrium* alone parasitizes amphibians (Joneson et al. 2011; Martel et

al. 2013; Berger et al. 1998). Expansions in peptidase, including *aspartyl*-, *M36 metallo*-, and *S41 serine-like peptidases*, have been observed in *Bd* compared to *Hp* (Joneson et al. 2011; Farrer et al. 2017). A class of *Crinkler Like Necrosis* (*CRN*) genes, thought to be specific to Oomycetes, are also found in abundance in the *Bd* reference genome and relatives (Joneson et al. 2011; Sun et al. 2011; James et al. 2013). Chitin Binding Module 18 Domain (CBM18) containing proteins, implicated in protecting fungal pathogens against host chitinases, are similarly noted to be expanded in *Bd* (Abramyan & Stajich 2012; Farrer et al. 2017). Additionally, peptidases, *CRNs* and *CBMs* appear to be up-regulated during *Bd* infection compared to when the fungus is grown on media, further implicating their role in pathogenicity (Rosenblum et al. 2012; Ellison et al. 2017). Recently a newly described species, *Polyrhizophydium stewartii* (*Ps*) has been identified and classified as a closer saprophytic relative of *Bd* than *Hp* (Simmons et al. 2021; Amses et al. 2022). The discovery of *Ps* provides a resource to improve understanding of the transition towards pathogenicity in chytrids. Genomic comparisons between *Ps* and *Bd* will expand upon previous comparisons between *Bd* and saprophytic chytrids.

Pangenomes are valuable tools to elucidate the genomic variation within a population. The mechanisms that allow *Bd*-GPL to globally proliferate while strains from other lineages remain endemic is not understood. Competition between *Bd* lineages, differences in virulence between *Bd*-GPL and endemic lineages, and unique genomic recombination in *Bd*-GPL have been demonstrated (Belasen et al. 2022; Jenkinson et al. 2016; Farrer et al. 2011). Here we utilized *Oxford Nanopore* Sequencing of three *Bd*-

BRAZIL strains and the species *Ps* JEL0888 to aid in the establishment of a *Bd* pangenome. In particular, our assembly of *Bd*-BRAZIL strain CLFT044 suggests an improvement on previous assemblies, possessing three telomere-to-telomere scaffolds. Furthermore the genome completeness estimates indicate that all three *Bd*-BRAZIL genomes are of similar quality to the previous assemblies, suggesting their utility in future genomic analysis. We present these new genomes to elucidate the genome content variability between *Bd*-GPL and *Bd-BRAZIL* strains.

Materials and Methods

DNA extraction

Three *Bd* strains from the *Bd*-BRAZIL lineage, CLFT044, CLFT067, and CLFT071, were grown on 1% Tryptone agar for seven days at 21°C. Zoospore and sporangia tissue was harvested from each culture by flooding with 1mL sterile reverse osmosis (RO) water, scraping colonies with an L-spreader, pelleted at 6500g for seven minutes, and flash frozen in liquid Nitrogen. *Ps* JEL0888 was grown in PmTG broth (1 g peptonized milk, 1 g tryptone, 5 g glucose, 1 L distilled water) for 14 days at 23°C before the samples were centrifuged at 6500g for seven minutes to remove broth and flash frozen in liquid Nitrogen. Cetyltrimethylammonium Bromide (CTAB) DNA extraction was performed on the frozen tissue samples from each isolate (Carter-House et al. 2020).

RNA extraction

Three biological replicates of three *Bd*-BRAZIL and two *Bd*-GPL strains were inoculated onto 1% Tryptone agar plates using 5 x 10^6 total active zoospores in 2mL of sterile RO water. Cultures were left to incubate under the same conditions as the DNA *Bd* tissue samples until active zoospores were visualized around every colony (5-7 days depending on the isolate). After incubation tissue samples were harvested with an L-spreader and pelleted at 6500g for seven minutes and flash-frozen in liquid nitrogen prior to RNA extraction. Because the samples were not filtered to remove sporangia, tissue samples consisted of both sporangia and zoospores. RNA was extracted from the tissue samples using TRIzol solution (*Invitrogen*, Mulgrave, VIC, Australia) under manufacturer's protocol coupled with an overnight precipitation in isopropanol at -21°C to increase yields. Total RNA was sent to *Novogene* (Davis, CA) for poly A enrichment, cDNA synthesis and *NovaSeq* PE150 sequencing to achieve 6Gb data per sample.

DNA sequencing

gDNA from the three *Bd*-BRAZIL strains was sent to *MiGS* (*SeqCenter*) for Oxford Nanopore Technologies (ONT) sequencing to obtain 900mbp reads (~30X coverage) for genome assembly. DNA from *Ps* JEL0888 was sequenced with the Oxford Nanopore MinION using the NBD104 barcoding kit and LSK109 ligation sequencing kit following manufacturer's protocols resulting in 696.915 Mb (~25X coverage).

Genome Assembly and Annotation

The ONT reads from all four samples were assembled *de novo* using *Canu* v2.2 (Koren et al. 2017) using the estimated genome size of 25Mb. *Canu* provided scaffolds with

telomeres but did not produce the most contiguous assemblies. Assembly was repeated with *MaSuRCA v4.0.9* (Zimin et al. 2013) incorporating publicly available Illumina sequence data for each strain (O'Hanlon et al. 2018; Amses et al. 2022) which produced a more consensus assembly. The *Canu* assemblies were scaffolded against their respective MaSuRCA assemblies with RAGTAG *v2.1.0* (Alonge et al. 2022) to achieve contiguous genomes with telomeres. The assemblies were polished by 10 iterations of *Pilon* v1.24 (Walker et al. 2014) run within AAFTF (Stajich & Palmer 2022) using publicly available Illumina sequence data (Rosenblum et al. 2013; Farrer et al. 2013; O'Hanlon et al. 2018; Amses et al. 2022; Clemons et al. 2023).

Annotation was performed using Funnanotate v1.8.14 (Palmer & Stajich 2023) utilizing the RNAseq data from the three *Bd*-BRAZIL strains to increase accuracy of gene predictions for those genomes. Briefly, this entailed sorting the scaffolds by size, RepeatMasker *v4.1.4* to mask the repetitive elements in the assemblies, training the *Bd*-BRAZIL assemblies with our RNAseq data, and functional annotation using default parameters. We downloaded the genome assemblies and annotations for three *Bd*-GPL strains; JEL423 (GCA_000149865), RTP6 (GCA_003595275.1) (Sumpter et al. 2018), and JAM81 (GCF_000203795) (Amses et al. 2022) to compare genomic content between BRAZIL and GPL strains.

We assessed the quality of our genome assemblies using QUAST v5.0.0 (Gurevich et al. 2013) and BUSCO v5.5.0 (Seppey et al. 2019) in genome mode against the fungi_odb10 gene sets. We compared the BUSCO and QUAST results with those from

the reference and high quality *Bd*-GPL genomes (supplementary table 1). We calculated telomere counts using pattern searching with find_telomeres.py (https://github.com/markhilt/genome_analysis_tools) to assess chromosome completeness for all assemblies. We used PHYling v2.0 (Stajich & Tsai) to generate a multi-gene alignment for phylogenetic analysis of *Bsal, Bd*, *Hp*, and *Ps* to confirm relatedness of strains and species. Phylogenic tree was constructed with RAxML v8.2.12 (Stamatakis 2014) and tree was rendered with ggtree v3.8.2 (Yu 2022).

Transposable Element Content

We used RepeatModeller *v2.0.4* (Flynn et al. 2020) and EDTA *v2.1.0* (Ou et al. 2022) to generate a library of transposable elements in the six *Bd* genome assemblies, *Ps, Hp,* and the *Batrachochytrium salamandrivorans* (*Bsal*) strain AMP13/1 (GCA_002006685.2) (Wacker et al. 2023). We merged the libraries generated from the different assemblies and collapsed out duplicate TEs using cd-hit *v4.8.1* at 98% ID (Huang et al. 2010). We used this condensed TE library and RepeatMasker *v4.1.5* (Smit et al. 2013-2022) to determine counts of LTR, LINE, and DNA TEs in the genomes. Unknown TEs were searched with BLASTN v2.14.1 (Altschul et al. 1997; Camacho et al. 2009) against *RepBase* (Bao et al. 2015) database to classify them as LTR *Copia*, *Gypsy*, or DNA Type II transposable elements.

Synteny analysis between representative *Bd*-BRAZIL and *Bd*-GPL strains

Scaffold synteny was estimated between the 10 longest scaffolds in *Bd*-BRAZIL strain CLFT044 against the *Bd*-GPL JEL423 *Sanger* and RTP6 *PacBio* genomes using

GENESPACE v1.2.0 (Lovell et al. 2022). The syntenic blocks between these three genomes were inferred using default settings, including *Ps* JEL0888 as the outgroup. The GENESPACE v1.2.0 riparian plot was constructed using JEL423 as the reference genome and flipping the orientation of CLFT044 scaffolds; scaffold_1, scaffold_2, scaffold_4, scaffold_5, and scaffold_8 which were inverted with respect to their RTP6 and JEL423 counterparts. We aligned the ONT DNA reads from CLFT044 back against the CLFT044 genome using minimap2 v2.24 (Li 2018) to confirm that reads supported merged scaffolds observed in CLFT044 but not JEL423 or RTP6.

Gene Family Variation between Bd and related species

We used Orthofinder *v2.5.4* (Emms & Kelly 2019) as an initial step towards comparative genomics by identifying gene families unique to the *Batrachochytrium* genus (*Bd* and *Bsal*), but absent in their saprophytic relatives. This included the three *Bd*-BRAZIL ONT-hybrid genomes and *Ps,* the three public *Bd*-GPL genomes; JEL423, JAM81, and the published PacBio *Bsal* genome APM13/1, and the Illumina genome for *Hp.* JEL423 gene IDs belonging to gene families specific to the pathogenic chytrids *Bd* and *Bsal* were searched against the *fungidb* database to identify Gene Ontology (GO) terms. Additionally we used Orthofinder to identify gene content differences between the three *Bd*-GPL and three *Bd*-BRAZIL long-read genomes to identify the core and pangenome of *Bd*. Orthofinder visualizations were rendered with UpsetR v1.4.0 (Conway et al. 2017).

Presence Absence Variation (PAV) of Pathogenicity genes in *Bd* and other chytrids

We performed HMMsearch 3.3.2 with an e-value of 1e-15 for PFAMs PF02128, PF03572, PF00026, and PF00187 to count the number of M36, S41, ASP, and CBM18 proteins respectively in each annotated genome (Eddy 2011). HMMsearches using the Crinkler necrosis (CRN) PFAM PF20147 were unsuccessful at detecting copies in *Bd*. We used HMMbuild on the previously identified CRN proteins in JEL423 to construct an hmm profile to screen and count CRN proteins in *Bd* strains (Farrer et al. 2017). We constructed a heatmap for the protein family counts using the R package pheatmap v.1.0.12 (Kolde 2019).

Since homologous genes are likely to be syntenic with homologs from closely related strains, we used Cblaster *v1.3.18* (Gilchrist et al. 2021) with a minimum percent identity of 80% and 2 flanking genes on the 5' and 3' end to identify the syntenic homologs of every *M36* and *CBM18* across the *Bd* strains. Genes were required to share the same four flanking genes, two upstream and two downstream of the *M36* or *CBM18*, to be considered homologous. This analysis identified the non-redundant set of orthologous *CBM18* or *M36* across all strains, preferentially using the JEL423 copies given its status as a primary reference genome. If orthologs were missing in JEL423, we represented them by a copy from another strain. We used MUSCLE *v5.1* (Edgar 2004) to align the non-homologous *M36* and *CBM18* encoding genes and constructed phylogenetic trees for both gene sets with IQTREE2 *v2.2.2.6 (Minh et al. 2020)* using the ModelFinder function which selected the VT+R10 model for *CBM18* and the TWM+F+R5 model for

M36 with 1000 SH-like bootstrap replicates (Kalyaanamoorthy et al. 2017). We included the *M36* and *CBM18* genes from *Hp* and *Ps* as outgroups and to root the phylogenies. Phylogenetic visualizations were rendered with the R package, ggtree v3.8.2 (Yu 2022).

CBM18 domain-containing proteins have been reported to contain multiple domains per gene in *Bd* strain JEL423 (Abramyan & Stajich 2012). The diversity of JEL423's CBM18 repertoire includes variable counts of Tyrosinase and Deacetylase domains, as well as Lectin-like CBM18 proteins without additional domains (Abramyan & Stajich 2012). We used HMMSCAN to catalog the variation in CBM18 domain copy number between CBM18 homologs in the *Bd* Long-read genomes (Eddy 2011).

RNAseq Read Mapping

Based on the genomic diversity we observed between *Bd* strains, we questioned the efficacy of using a single reference genome for transcriptomic analysis of different *Bd* strains. To assess whether a *Bd*-BRAZIL reference genome will increase recovery of *Bd*-BRAZIL transcripts, we aligned RNAseq reads from four *Bd*-BRAZIL and two *Bd*-GPL strains were aligned to the *Bd*-BRAZIL CLFT044 assembly and to the *Bd*-GPL genome for JEL423 (GCA_000149865) using HISAT2 *v2.2.1 (Kim et al. 2019)*. All sequence reads were mapped to the indexed genomes. Raw read counts were generated with FeatureCounts from Rsubread (Liao et al. 2019) and TPM values were calculated with edgeR (Robinson et al. 2010). Given the genetic variation between *Bd* strains, we tested how much the reference genome matters when calculating gene expression in *Bd* RNAseq data. We aligned the three replicates of PE RNAseq reads

from CLFT044 against the CLFT044 genome and against the JEL423 genome to calculate the ratio of TPMs when aligning to CLFT044 (self) over JEL423 (ref). We focused this analysis on Single-Copy orthologous gene families, genes determined from Orthofinder to be single copy in both genomes, to avoid ambiguity caused by comparing distant orthologs. Using a global-pairwise sequence alignment of the two orthologous coding sequences (Pearson 2000) we scored sequence pairs for their alignability and then evaluated the relationship of sequence divergence, number of secondary blast hits, gap openings, and mismatch differences between CLFT044 and JEL423 to test whether length or sequence differences between homologous genes explain the variation in TPM calculations.

We tested whether genomic differences have inflated the number of differentially expressed genes (DEGs) between *Bd*-BRAZIL and *Bd*-GPL strains. A previous study reported DEGs between the *Bd*-BRAZIL and *Bd*-GPL lineages when RNA from two *Bd*-BRAZIL strains (CLFT044 and CLFT001) and four *Bd*-GPL strains (CLFT023, CLFT026, JEL410, and JEL422) are aligned to the reference genome strain JEL423 (McDonald et al. 2020). We performed HISAT2 alignments of the RNAseq data from this study to the reference genome of strain JEL423 and separately aligned to CLFT044. We used the R packages FeatureCounts and DeSeq2 *v*1.4.2 (Love et al. 2014) to re-calculate the number of differentially expressed genes (log2fold $\geq$ 1.5 and Bonferroni adjusted p-value $\leq$ 0.05) between the *Bd*-BRAZIL and *Bd*-GPL lineages. We intersected the identities of differentially expressed genes with the identities of *Bd*-GPL /*Bd*-BRAZIL specific genes from Orthofinder and the identities of the single copy

orthologous genes with reference dependent transcript counts. Images depicting this intersection were rendered using the R package ggvenn *v.* 0.1.10 (Yan).

Results

Assembly quality of *Bd*-BRAZIL genomes is comparable to that of the reference genomes

The *Bd*-BRAZIL genomes were assessed to be of similar quality to the three published GPL genomes in measures of total contig count, N50, and BUSCO completeness (supplementary table 1). After assembly the *Bd*-BRAZIL genome assemblies composed 79, 86, and 85 contigs for CLFT044, CLFT067, and CLFT071 respectively with total lengths between 22Mb and 26Mb. BUSCO assessment of the assemblies concluded similar scores with average completeness for all *Bd*-BRAZIL genomes at 89.9% against the fungi_odb10 gene sets, slightly higher than the reference genomes JEL423 and JAM81. The assembly of *Ps* JEL0888 contained 291 scaffolds with an average BUSCO completeness of 81.4%. The *Ps* genome assembly was slightly larger than all the *Bd* assemblies at 31Mb. The *Hp* assembly (GCA_000235945.1) was far less contiguous and complete than those of the other chytrids, being assembled exclusively from short-read sequencing data. The *Hp* assembly possesses 11986 scaffolds and a BUSCO completeness of 80.9. Furthermore its largest scaffold was only 227.1kb long, far shorter than the largest scaffolds of the other chytrid assemblies.

Synteny is conserved along the 10 largest scaffolds between CLFT044 and the GPL reference genomes

Conserved syntenic regions between the longest 10 scaffolds in *Bd*-BRAZIL strain CLFT044 were compared with their homologs in *Bd*-GPL strains JEL423 and RTP6 (**Figure 2**). The 10 largest scaffolds in CLFT044 were present in the RTP6 and JEL423 assemblies. Scaffold_5 and Scaffold_9 appear to be split in CLFT044, being combined as DS022301.1 and QUAD01000002.1 in JEL423 and RTP6 respectively. Scaffold_5 contains one telomere on the 5' end while Scaffold_9 does not possess telomeric sequences. This suggests completeness on the 5' end of this region while the center and 3' ends of the chromosome were not contiguously assembled.

Scaffold_2 in CLFT044 represents a more contiguous assembly, being a merge of the two contigs DS022302.1 and DS022309.1 in JEL423. ONT reads from CLFT044 spanned the entire Scaffold_2 region, indicating the validity of this merged scaffold compared to other assemblies.

Scaffold_3, Scaffold_4, and Scaffold_6 in CLFT044 all contained forward and reverse telomeres based on the telomere search results suggesting their status as complete chromosome assemblies. Although Scaffold_4 in CLFT044 is likely a complete chromosomal assembly, its homolog extends farther on the 5' end in JEL423 and RTP6. This difference in length could be due to genome size differences between strains rather than assembly quality.

Bd* is expanded in genome size and TE content to *Hp* but reduced compared to *Ps

Bd-BRAZIL and *Bd-GPL* strains were overall similar in genome size, genic space, and TE content (**Figure 1**). The *Bd*-BRAZIL strain, CLFT044 alone possesses an abundance of LTR elements and DNA transposons compared to the other strains. Our results support previous findings that *Hp* has a reduced genome size and TE content compared to *Bd (Farrer et al. 2017).*

The gene counts found in all *Bd* strains were higher than the count in *Hp,* however *Ps* possesses a greater number of genes than any of the *Bd* strains. All other species were dwarfed in gene count compared to *Bsal* while overall gene counts were mostly similar between the *Bd* genomes.

TE expansion has been suggested as a driving force in the acquisition of pathogenicity genes in *Batrachochytrium (Wacker et al. 2023)*. We identified expansions in LTR, LINE, and DNA transposable elements in *Bd* and *Bsal* compared to *Hp. Ps* was expanded in LTR and LINE elements compared to *Bd*, however its genome contains fewer DNA TEs than any of the *Bd* strains. All *Bd* strains are expanded in DNA TEs compared to the other species including *Bsal*.

***Bd*-BRAZIL and *Bd*-GPL possess many lineage specific gene families**

Analysis of shared orthogroups between *Bd* and closely related species (**Figure 3A**) reveals 348 gene families that are distinct to the *Batrachochytrium* genus (all *Bd* strains and *Bsal*), but absent in the saprophytic chytrids. Additionally 435 gene families were

unique to *Bd*, being present in all *Bd* strains but absent in the other chytrid species. GO analysis on the JEL423 genes found in the pathogen specific gene families indicates pathogen specific expansions in *Metallopeptidase* gene families (**Supplemental figure S2**).

Orthofinder results between *Bd* strains indicate that there are 6278 core gene families in the *Bd* pangenome (**Figure 3B**). We identified 1,934 accessory gene families that were present in two or more strains and 160 singletons present in single strains. Among the accessory gene families, we find 202 to be distinct to the *Bd*-BRAZIL strains while 172 are unique to *Bd*-GPL. The singletons are unequally divided among strains with strains JEL423 and JAM81 having the highest number of unique gene families (51 and 50 respectively) while the remaining strains each possessed only 10-30 singleton gene families. We identified a gene family of putative Meiotically up-regulated gene 113 (mug113) proteins found in other fungi and in the *Bd*-BRAZIL lineage but absent in *Bd*-GPL. Among the *Bd*-GPL specific gene families were many proteins of unknown function that were absent in all *Bd*-BRAZIL strains. Interestingly the reference genome strains JEL423 and JAM81 lacked 105 gene families that are present in all the other *Bd* genomes (**Supplementary figure S3**).

Pathogenicity genes vary in count and sequence between *Bd* strains and other chytrids

Our HMMsearch analysis of the five pathogenicity genes revealed variation in copy number and sequence diversity of these gene families among *Bd* strains and sister

species (**Figure 4)**. Among the putative pathogenicity genes, all *Bd* strains were expanded in copy number for S41 Peptidase, ASP protease, CBM18, and CRN relative to saprophytic chytrids. CRN had the highest observed expansion in *Bd* compared to its saprophytic relatives which ranged from one to six copies in *Hp* and *Ps* and 27-108 copies in the *Bd* strains. Although we observed variation in pathogenicity gene count variation between *Bd* strains, the genes were not consistently expanded in *Bd*-GPL over *Bd*-BRAZIL. We compared the pathogenicity gene counts detected in long-read genomes with the counts found in the annotated genome of Illumina-only short read genomes for the same strains to determine whether sequencing technology plays a significant role in capturing Pathogenicity gene diversity (**Supplementary figure S4**). While counts for the *SWEET* and *Adenylate kinase* gene families were consistent between Illumina and Long-read genomes, the pathogenicity genes were consistently under-represented in the Illumina assemblies compared to the long-read genomes for the same strain.

Using cblaster we resolved *M36* and *CBM18* genes into orthologous loci using flanking syntenic genes. To identify core, variable, and singleton *M36* and *CBM18* genes in the *Bd* pangenome we allowed co-located homologous sequences found in multiple strains to be represented by an ortholog from a single strain. We searched with cblaster to find these representative orthologs in the *Bd* pangenome and determine the distribution of core and variable *CBM18s* and M36*s* in the *Bd* pangenome. If the core or variable *M36/CBM18* was found in JEL423, the representative was named with the JEL423 copy, otherwise it was named for the representative from another *Bd* strain. Prior to

collapsing duplicate orthologs there were a total of 210 *M36* and 91 *CBM18* copies in all six *Bd* strains. Collapsing the orthologous copies from separate strains resulted in 59 and 20 unique orthologs of *M36* and *CBM18* respectively.

Phylogenetic analyses of the *M36* orthologs revealed ancestral and *Bd* exclusive clades of *M36* (**Figure 5A**). Despite similar counts of *M36* genes between *Ps* and *Bd*, the copies from both species, we observed sequence level variation that segregated the *M36* orthologs from the *Ps* orthologs. We defined the ancestral M36 clade as the clade of *M36* orthologs that contained members of *M36* found in all genomes and species while the *Bd* specific clade contains orthologs found only in *Bd*. Furthermore we identified a previously unknown clade of *M36* genes unique to *Ps. Bsal*'s *M36* repertoire is expanded compared to *Bd,* with two clades of *Bsal* specific *M36* clades sister to the *Bd* specific clade (**Supplementary figure S5**). *Bsal* and *Bd* possess similar counts of *M36* genes in the ancestral *M36* clade with three copies in *Bsal* and six in *Bd*.

We searched with cblaster for the newly identified *M36* ortholog clusters against the six Long-read *Bd* genomes to establish the conservation of these *M36* orthologs across the *Bd* strains (**Figure 5B**). We identified 15 core *M36* orthologs conserved in all six genomes. While we did not identify any *Bd*-GPL specific *M36* orthologs we discovered two *Bd*-BRAZIL specific *M36* clusters that were present in two-three *Bd*-BRAZIL strains but absent in all *Bd*-GPL. Additionally we reveal the presence of nine *M36* singletons, present in only single strains. We analyzed the region of MT418_006102, a singleton *M36* from *Bd*-BRAZIL strain CLFT044, and compared its syntenic structure to its closest

relative BDEG_24855, a core *M36* from the ancestral clade. We discovered that the flanking region of MT418_006102 was duplicated and downstream of the BDEG_24855 syntenic cluster in CLFT044 (**Supplementary figure S6**).

Annotation error has likely contributed to the *M36* count variation between *Bd* strains. Cblaster analysis revealed the JEL423 gene BDEG_27858 to be orthologous with a pair of tandem *M36* genes in all other strains (**Supplementary figure S7**). The combined length of the *M36* pair in other strains was equal to the length of BDEG_27858 further suggesting the genes were erroneously merged during annotation of the reference genome. One of the *M36* loci in this region was likewise fragmented in JAM81 resulting in three *M36* genes rather than two.

We identified variation in the domain content of *CBM18* genes between *Bd*, *Ps*, and *Hp* (**Figure 6A**). *Bd* and *Hp* both possess only one copy of Tyrosinase containing CBM18 proteins while *Ps* contains three that are co-localized, possibly a result of tandem duplication. Lectin-like CBM18 proteins were expanded in *Bd* compared to either of its relative species, with only two present in *Ps*, none in *Hp,* and 10-14 orthologs in each *Bd* strain. Additionally we discovered differences in CBM18 Domain counts within homologs between the *Bd* strains (**Figure 6B).** We found that most CBM18 homologs (with the exception of BDEG_23733) varied in CBM18 domain count between different strains*.* One example displaying such diversity was BDEG_21734 which contains five domain copies in all *Bd*-GPL strains and four per *Bd*-BRAZIL. Furthermore, homologs of BDEG_20255 which, although present and syntenic in all *Bd* genomes, varied

significantly in CBM18 domain counts with three to five domains per strain (**Supplementary figure S8)**.

Aligning transcripts from *Bd*-BRAZIL strains to JEL423 may under or over-estimate gene expression for some genes

Our HISAT2 alignment revealed that transcripts from Bd-BRAZIL strains aligned back to the CLFT044 genome at an average rate of 97.52 and to the JEL423 genome at 96.85. We found that overall, the TPM ratios for CLFT044 transcripts when aligned to CLFT044 vs. JEL423 varied little, with the average TPM ratio at approximately 1 (0.993) (**Figure 7B)**. Despite the largely consistent average, we found that the CLFT044 transcripts from 145 Single Copy genes are under-represented (TPM ratio > 1.2) and 279 are over-represented (TPM ratio < 0.79) when aligning to the JEL423 genome (**Figure 7C**). Gene length variance, percent ID, and number of secondary blast hits between JEL423 and CLFT044 were significantly correlated to TPM variance, however we were unable to determine a conclusive cause for this variance (**Supplementary figure 8**).

Differential expression analysis using RNAseq data from a previous study (McDonald et al. 2020) revealed 1083 DEGs between the *Bd*-BRAZIL and *Bd*-GPL lineages using JEL423 as the reference genome. Among these DEGs, 89 genes were specific to the *Bd*-GPL lineage, 43 were among the single-copy orthologous genes identified as over or under-represented when aligning RNA to the JEL423 reference genome (**Supplementary figure 10A**). Aligning the same RNAseq data to the CLFT044 genome

resulted in 788 DEGs. 31 of the DEGs were *Bd*-BRAZIL specific genes and 49 were genes with reference dependent transcript counts (**Supplementary figure 10B**).

Discussion

Bd is the causative agent of chytridiomycosis in amphibian populations around the world, including North and South America (Longcore et al. 1999). However, the pathogen is not a monolith, as strains from different lineages exhibit variable distribution and virulence on their amphibian hosts (Dang et al. 2017; Rosenblum et al. 2013). Little is known about the functional differences that drive pathogenicity variance between the *Bd*-GPL and *Bd*-BRAZIL lineages; therefore these new *Bd*-BRAZIL genomes represent a valuable dataset through which to examine this variance. Although genome expansions and TE invasions have been implied as a driving force in hypervirulence between some strains of plant pathogenic fungi (Grandaubert et al. 2014) we did not detect an abundance of TEs in *Bd*-GPL strains compared to *Bd*-BRAZIL. Similarly our counts of pathogenicity genes between *Bd* strains reveals that there is no clear case of *Bd*-GPL consistently possessing more members of a pathogenicity gene family, however there exists intense copy number variation of pathogenicity genes between *Bd* strains.

We observed sequence level variation between *Bd* and *Ps M36* genes despite overall similarity in *M36* counts between the two species. Phylogenetic analysis revealed an ancestral clade of *M36* with copies from *Bd*, *Ps*, *Bsal*, and *Hp* as well as a clade of *M36* genes exclusive to *Bd*. While the ancestral *M36* genes were universally present among the *Bd*-BRAZIL and *Bd*-GPL lineages, the *Bd* exclusive *M36* genes were

more variable in presence/absence among the *Bd* genomes. Furthermore we detected 23 *M36* genes from *Bd*-BRAZIL genomes without homologs in the reference genome JEL423, illustrating the breadth of gene family diversity that is lost while relying upon a single reference genome. Two of the newly discovered *M36* loci in *Bd* were co-localized and shared high sequence similarity with conserved *M36* genes, suggesting they may have arisen from tandem duplication.

Along with overall gains and losses in pathogenicity gene content between *Bd* strains, we observe diversity in domain counts within homologs of the CBM18 protein family. The phenomenon of domain gains and losses within a single protein is rare yet has been previously reported in other systems (Prakash & Bateman 2015). In one CBM18 ortholog (BDEG_21734) we note a consistent domain gain from four to five domains between *Bd*-GPL and *Bd*-BRAZIL strains. It is possible that such changes in protein structure could affect the functions of these homologs, however this can not be proven without strenuous functional analysis.

Studies have focused on the genomic repertoire of reference genomes JEL423 and JAM81, however we show that there is a breadth of genomic diversity that is lost when relying on a single reference genome. Previous work on gene expression variance between *Bd*-BRAZIL and *Bd*-GPL strains has been conducted by aligning transcripts to the JEL423 genome, indicating an up-regulation of some pathogenicity genes in *Bd*-GPL with respect to *Bd*-BRAZIL strains (McDonald et al. 2020)**.** Our transcriptome analysis of CLFT044 transcripts aligned against the CLFT044 and JEL423 genomes suggests that, although mostly accurate, transcription will likely be over or under-estimated for many genes. The results of our differential expression

analysis between *Bd*-BRAZIL and *Bd*-GPL lineages suggests that genomic differences (lineage specific gene families and genes with reference dependent transcript counts) could explain ~12.8% of the DEGs identified. Additionally we determined that aligning RNA from *Bd*-BRAZIL isolates to the JEL423 assembly will recover ~2% fewer reads than when aligning to CLFT044. We therefore suggest a candidate reference genome for every *Bd* lineage to more accurately assess future transcriptomic comparisons. While our analysis elucidated a partial pangenome between *Bd*-BRAZIL and the hyper-pathogenic *Bd*-GPL strains, it does not include representatives from *Bd*-CAPE and *Bd*-ASIA lineages. Although there are Illumina genomes for strains from these lineages, high-quality long-read assemblies for these genomes are currently unavailable nor did we have access to those strains for deep sequencing. Additionally Illumina *Bd* assemblies were not comparable to the long-read genomes as they did not capture the full diversity of multi-copy gene families, such as pathogenicity genes. Future studies including high quality long-read genomes from all lineages will improve upon the *Bd* pangenome analysis that we report here. We hope these genomic resources will help future exploration of genomic variation in *Bd,* potentially elucidating the mechanisms that make *Bd*-GPL a more globally successful pathogen than the other lineages.

Data Availability

The primary sequence data for Nanopore and Illumina DNA sequencing data are under BioProjects PRJNA987700 (*Polyrhizophydium stewartii* JEL0888), PRJNA987741 (*Batrachochytrium dendrobatidis* CLFT067), CLFT044 [XX]. RNA sequencing data are deposited under the accession numbers GSE253912 and GSE246809.

Acknowledgements

JES is a Fellow in CIFAR program Fungal Kingdom: Threats and Opportunities. The work was partially supported by a catalyst grant from CIFAR and CIFAR fellowship funds and U.S. Department of Agriculture, National Institute of Food and Agriculture Hatch projects CA-R-PPA-211-5062-H. The Gordon and Betty Moore Foundation Award #9337 (10.37807/GBMF9337) to Lilian Fritz-Laylin (PI), Timothy Y James, and Jason Stajich supported Mark Yacoub. Genome assembly and annotation were performed on the IIGB High-Performance Computing Cluster supported by NSF DBI-1429826, DBI-2215705, and NIH S10-OD016290 grants. We thank Dr. Timothy Y. James and the culture contributors of the Collection of Zoosporic EuFungi of Michigan (CZEUM) for providing the *Bd*-BRAZIL and *Ps* isolates used in this study. We would also like to thank Dr. Timothy Y. James, Dr. Cassie Ettinger, Dr. Tania Kurbessoian, Dr. Jessica Huang, Kian Kelly, and Julia Adams for helpful suggestions on this manuscript.

Figure Legends

Figure 1: Variation in overall the total length, gene counts, repeat TE counts between *Bd* strains, *Bsal*, *Hp*, and *Ps*. (Left) A barplot is shown depicting the length in Mbp of overall genome size (purple), genic space (green), non-repeat intergenic space (red), and TE content (blue). (Middle) Gene counts in the genomes are shown in the gold barplot. Scale is in number of genes. (Right) TE counts are represented by the blue barplot. TEs were classified as either DNA, LTR, or LINE elements.

Figure 2: A Riparian plot generated by GENESPACE v1.2.0 depicting synteny between scaffolds in CLFT044, JEL423, and RTP6. Orthology was used to visualize and compare synteny between the 10 longest scaffolds in CLFT044 and their homologs in RTP6 and JEL423. Genomes are organized by row and scaffolds are organized by column. Linkages are color coded by their respective scaffold in the reference genome JEL423. Telomeres are depicted as blue circles on the scaffold labels.

Figure 3: Orthofinder Pangenome analysis between chytrid species and between *Bd* strains visualized as Upset plots. (A) Upset plot depicting Orthofinder results for six *Bd* strains and related species *Bsal, Ps, and Hp* and (B) between *Bd* strains only. Vertical bars display the counts of gene families in each group while the dots indicate the strains present in each group. Only accessory and singleton gene families are shown. Gene families found in a single strain are indicated as a single dot and colored by strain.

Figure 4: Copy number variation for pathogenicity genes *CBM18, M36, S41, ASP*, and *CRN* between *Bd* and saprophytic chytrids. A heatmap is shown depicting the copy number variation of pathogenicity genes (SWEET and Adenylate Kinase included as controls). The colors of the tiles represent log2fold difference from the average and are normalized per gene family with red and blue indicating high and low counts respectively. The sequencing technology used to produce each genome is shown by the gray-scale bar while the top color bar indicates the species for each strain.

Figure 5: Phylogenetic relationships and distribution of *Bd* exclusive *M36* loci and those from saprophytic chytrids. (A) Maximum likelihood phylogeny inferred by IQTREE of the unique *M36* genes in *Bd*, *Hp,* and *Ps* is depicted here. Duplicate orthologs are collapsed by results from cblaster. Tips are color coded based on the species that M36 homolog is found in. The clade of *M36* genes exclusive to *Bd* is labeled in red and the ancestral clade containing representative *M36* genes from all species is labeled in blue. SH-like support values are color-coded at the nodes. (B) Phylogeny of unique M36 orthologs and their presence/absence in the six *Bd* genomes. A reduced *M36* tree from figure 5A, focused on *M36* from only *Bd.* The SH-like support values are color coded on the branches. The heatmap represents the percentage of Illumina genomes in each lineage that contain that M36 homolog. The ancestral M36 clade is labeled.

Figure 6: Homologous *CBM18* genes display variable domain counts between *Bd* strains. Maximum-likelihood *CBM18* whole gene phylogeny inferred by IQTREE with duplicate orthologs collapsed based on blaster results from *Bd, Ps*, and *Hp.* Clade labels define genes within each clade by class; Tyrosinase, Deacetylase, and Lectin-like. Tree tips are coded by species. In association with the tree tips, a heatmap depicts domain counts for that CBM18 homolog. Columns of the heatmap indicate the genomes of *Hp, Ps,* and the long-read *Bd* genomes. White colors indicate low-counts of CBM18 domains for the homolog in that genome. Red indicates that strain has a high count of CBM18 domains in that protein. Gray indicates the absence of the entire CBM18 homolog.

Figure 7: *Bd* reference genome affects recovery and alignment of RNAseq transcripts. Alignment of *Bd*-BRAZIL strain transcripts to CLFT044 and JEL423**.** (A) The percentage of aligned transcripts from four *Bd*-BRAZIL strains and two *Bd*-GPL strains to the reference genomes CLFT044 and JEL423 is shown. X-axis indicates the RNAseq donor strain. Gold x-axis labels indicate the RNAseq donor strains from the *Bd*-BRAZIL lineage and purple labels are strains from *Bd*-GPL. Boxplots are color coded by reference genome. (B) A dotplot is shown depicting the TPM ratio for CLFT044 RNAseq data when aligned to the CLFT044 genome versus aligning to the JEL423 genome for the single-copy orthologous genes. Each gold point represents a single copy ortholog gene and the y-axis represents the ratio of TPM when aligned to CLFT044 over JEL423. The green line/dot represents the average TPM ratio (0.993). (C) The number of genes with TPM ratios below (red), within (green), and above one (blue) SD of “one”. Genes with transcripts within the green class are accurately counted regardless of reference genome.

Abramyan J, Stajich JE. 2012. Species-specific chitin-binding module 18 expansion in the amphibian pathogen *Batrachochytrium dendrobatidis*. MBio. 3:e00150–12.

Alonge M et al. 2022. Automated assembly scaffolding using RagTag elevates a new tomato system for high-throughput genome editing. Genome Biol. 23:258.

Altschul SF et al. 1997. Gapped BLAST and PSI-BLAST: a new generation of protein database search programs. Nucleic Acids Res. 25:3389–3402.

Amses KR et al. 2022. Diploid-dominant life cycles characterize the early evolution of Fungi. Proc. Natl. Acad. Sci. U. S. A. 119:e2116841119.

Bao W, Kojima KK, Kohany O. 2015. Repbase Update, a database of repetitive elements in eukaryotic genomes. Mob. DNA. 6:11.

Becker CG et al. 2017. Variation in phenotype and virulence among enzootic and panzootic amphibian chytrid lineages. Fungal Ecol. 26:45–50.

Belasen AM, Russell ID, Zamudio KR, Bletz MC. 2022. Endemic Lineages of *Batrachochytrium dendrobatidis* Are Associated With Reduced Chytridiomycosis-Induced Mortality in Amphibians: Evidence From a Meta-Analysis of Experimental Infection Studies. Frontiers in Veterinary Science. 9:756686.

Berger L et al. 1998. Chytridiomycosis causes amphibian mortality associated with population declines in the rain forests of Australia and Central America. Proc. Natl. Acad. Sci. U. S. A. 95:9031–9036.

Byrne AQ et al. 2019. Cryptic diversity of a widespread global pathogen reveals expanded threats to amphibian conservation. Proc. Natl. Acad. Sci. U. S. A. 116:20382–20387.

Camacho C et al. 2009. BLAST+: architecture and applications. BMC Bioinformatics. 10:421.

Carter-House D, Stajich JE, Unruh S, Kurbessoian T. 2020. Fungal CTAB DNA extraction. Protocols.io. doi: 10.17504/protocols.io.bhx8j7rw.

Clemons R et al. 2023. DNA virus BdDV-1 of the amphibian pathogen *Batrachochytrium dendrobatidis* is associated with hypervirulence. bioRxiv. 2023.03.16.532857. doi: 10.1101/2023.03.16.532857.

Conway JR, Lex A, Gehlenborg N. 2017. UpSetR: an R package for the visualization of intersecting sets and their properties. Bioinformatics. 33:2938–2940.

Dang TD, Searle CL, Blaustein AR. 2017. Virulence variation among strains of the emerging infectious fungus *Batrachochytrium dendrobatidis* (Bd) in multiple amphibian host species. Dis. Aquat. Organ. 124:233–239.

Daszak P et al. 1999. Emerging infectious diseases and amphibian population declines. Emerg. Infect. Dis. 5:735–748.

Eddy SR. 2011. Accelerated Profile HMM Searches. PLoS Comput. Biol. 7:e1002195.

Edgar RC. 2004. MUSCLE: multiple sequence alignment with high accuracy and high throughput. Nucleic Acids Res. 32:1792–1797.

Ellison AR, DiRenzo GV, McDonald CA, Lips KR, Zamudio KR. 2017. First *in Vivo Batrachochytrium dendrobatidis* Transcriptomes Reveal Mechanisms of Host Exploitation, Host-Specific Gene Expression, and Expressed Genotype Shifts. G3. 7:269–278.

Emms DM, Kelly S. 2019. OrthoFinder: phylogenetic orthology inference for comparative genomics. Genome Biol. 20:238.

Farrer RA et al. 2013. Chromosomal copy number variation, selection and uneven rates of recombination reveal cryptic genome diversity linked to pathogenicity. PLoS Genet. 9:e1003703.

Farrer RA et al. 2017. Genomic innovations linked to infection strategies across emerging pathogenic chytrid fungi. Nat. Commun. 8:14742.

Farrer RA et al. 2011. Multiple emergences of genetically diverse amphibian-infecting chytrids include a globalized hypervirulent recombinant lineage. Proc. Natl. Acad. Sci. U. S. A. 108:18732–18736.

Flynn JM et al. 2020. RepeatModeler2 for automated genomic discovery of transposable element families. Proc. Natl. Acad. Sci. U. S. A. 117:9451–9457.

Gilchrist CLM et al. 2021. cblaster: a remote search tool for rapid identification and visualization of homologous gene clusters. Bioinform Adv. 1:vbab016.

Grandaubert J et al. 2014. Transposable element-assisted evolution and adaptation to host plant within the *Leptosphaeria maculans-Leptosphaeria biglobosa* species complex of fungal pathogens. BMC Genomics. 15:891.

Greenspan SE et al. 2018. Hybrids of amphibian chytrid show high virulence in native hosts. Sci. Rep. 8:9600.

Gurevich A, Saveliev V, Vyahhi N, Tesler G. 2013. QUAST: quality assessment tool for genome assemblies. Bioinformatics. 29:1072–1075.

Huang Y, Niu B, Gao Y, Fu L, Li W. 2010. CD-HIT Suite: a web server for clustering and comparing biological sequences. Bioinformatics. 26:680–682.

James TY et al. 2013. Shared signatures of parasitism and phylogenomics unite Cryptomycota and microsporidia. Curr. Biol. 23:1548–1553.

Jenkinson TS et al. 2016. Amphibian-killing chytrid in Brazil comprises both locally endemic and globally expanding populations. Mol. Ecol. 25:2978–2996.

Joneson S, Stajich JE, Shiu S-H, Rosenblum EB. 2011. Genomic transition to pathogenicity in chytrid fungi. PLoS Pathog. 7:e1002338.

Kalyaanamoorthy S, Minh BQ, Wong TKF, von Haeseler A, Jermiin LS. 2017. ModelFinder: fast model selection for accurate phylogenetic estimates. Nat. Methods. 14:587–589.

Kilpatrick AM, Briggs CJ, Daszak P. 2010. The ecology and impact of chytridiomycosis: an emerging disease of amphibians. Trends Ecol. Evol. 25:109–118.

Kim D, Paggi JM, Park C, Bennett C, Salzberg SL. 2019. Graph-based genome alignment and genotyping with HISAT2 and HISAT-genotype. Nat. Biotechnol. 37:907–915.

Kolde R. 2019. pheatmap: Pretty Heatmaps. R package version 1.0. 12.

Koren S et al. 2017. Canu: scalable and accurate long-read assembly via adaptive k-mer weighting and repeat separation. Genome Res. 27:722–736.

Liao Y, Smyth GK, Shi W. 2019. The R package Rsubread is easier, faster, cheaper and better for alignment and quantification of RNA sequencing reads. Nucleic Acids Res. 47:e47.

Li H. 2018. Minimap2: pairwise alignment for nucleotide sequences. Bioinformatics. 34:3094–3100.

Longcore JE, Pessier AP, Nichols DK. 1999. *Batrachochytrium dendrobatidis* gen. et sp. nov., a chytrid pathogenic to amphibians. Mycologia. 91:219–227.

Lovell JT et al. 2022. GENESPACE tracks regions of interest and gene copy number variation across multiple genomes. eLife. 11:e78526.

Love MI, Huber W, Anders S. 2014. Moderated estimation of fold change and dispersion for RNA-seq data with DESeq2. Genome Biol. 15:550.

Martel A et al. 2013. *Batrachochytrium salamandrivorans* sp. nov. causes lethal chytridiomycosis in amphibians. Proc. Natl. Acad. Sci. U. S. A. 110:15325–15329.

McDonald CA, Ellison AR, Toledo LF, James TY, Zamudio KR. 2020. Gene expression varies within and between enzootic and epizootic lineages of *Batrachochytrium dendrobatidis* (Bd) in the Americas. Fungal Biol. 124:34–43.

Minh BQ et al. 2020. IQ-TREE 2: New Models and Efficient Methods for Phylogenetic Inference in the Genomic Era. Mol. Biol. Evol. 37:1530–1534.

O'Hanlon SJ et al. 2018. Recent Asian origin of chytrid fungi causing global amphibian declines. Science. 360:621–627.

Ou S et al. 2022. Benchmarking transposable element annotation methods for creation of a streamlined, comprehensive pipeline. Genome Biol. 20:275.

Palmer JM, Stajich JE. 2023. *Funannotate: Eukaryotic genome annotation*. doi: 10.5281/zenodo.4054262.

Pearson WR. 2000. Flexible sequence similarity searching with the FASTA3 program package. Methods Mol. Biol. 132:185–219.

Prakash A, Bateman A. 2015. Domain atrophy creates rare cases of functional partial protein domains. Genome Biol. 16:88.

Robinson MD, McCarthy DJ, Smyth GK. 2010. edgeR: a Bioconductor package for differential expression analysis of digital gene expression data. Bioinformatics. 26:139–140.

Rosenblum EB et al. 2013. Complex history of the amphibian-killing chytrid fungus revealed with genome resequencing data. Proceedings of the National Academy of Sciences. 110:9385–9390.

Rosenblum EB, Poorten TJ, Joneson S, Settles M. 2012. Substrate-specific gene expression in *Batrachochytrium dendrobatidis*, the chytrid pathogen of amphibians. PLoS One. 7:e49924.

Scheele BC et al. 2019. Amphibian fungal panzootic causes catastrophic and ongoing loss of biodiversity. Science. 363:1459–1463.

Schloegel LM et al. 2012. Novel, panzootic and hybrid genotypes of amphibian chytridiomycosis associated with the bullfrog trade. Mol. Ecol. 21:5162–5177.

Seppey M, Manni M, Zdobnov EM. 2019. BUSCO: Assessing Genome Assembly and Annotation Completeness. Methods Mol. Biol. 1962:227–245.

Simmons DR, Longcore JE, James TY. 2021. *Polyrhizophydium stewartii*, the first known rhizomycelial genus and species in the Rhizophydiales, is closely related to *Batrachochytrium*. Mycologia. 113:684–690.

Smit AFA, Hubley R, Green P. 2013-2022. *RepeatMasker Open-4.0*. http://www.repeatmasker.org.

Stajich JE, Palmer J. 2022. *AAFTF: Automatic Assembly For The Fungi*. doi: 10.5281/zenodo.7439973.

Stajich J, Tsai C-H. *PHYling for Phylogenomic reconstruction from genomes*. doi: 10.5281/zenodo.10147706.

Stamatakis A. 2014. RAxML version 8: a tool for phylogenetic analysis and post-analysis of large phylogenies. Bioinformatics. 30:1312–1313.

Sumpter N, Butler M, Poulter R. 2018. Single-Phase PacBio De Novo Assembly of the Genome of the Chytrid Fungus *Batrachochytrium dendrobatidis*, a Pathogen of Amphibians. Microbiol Resour Announc. 7:e01348–18.

Sun G, Yang Z, Kosch T, Summers K, Huang J. 2011. Evidence for acquisition of virulence effectors in pathogenic chytrids. BMC Evol. Biol. 11:195.

Wacker T et al. 2023. Two-speed genome evolution drives pathogenicity in fungal pathogens of animals. Proc. Natl. Acad. Sci. U. S. A. 120:e2212633120.

Walker BJ et al. 2014. Pilon: an integrated tool for comprehensive microbial variant detection and genome assembly improvement. PLoS One. 9:e112963.

Yan L. ggvenn: Draw Venn Diagram by ‘ggplot2’. R Package Version.

Yu G. 2022. *Data Integration, Manipulation and Visualization of Phylogenetic Trees*. CRC Press, Taylor & Francis Group.

Zimin AV et al. 2013. The MaSuRCA genome assembler. Bioinformatics. 29:2669–2677.

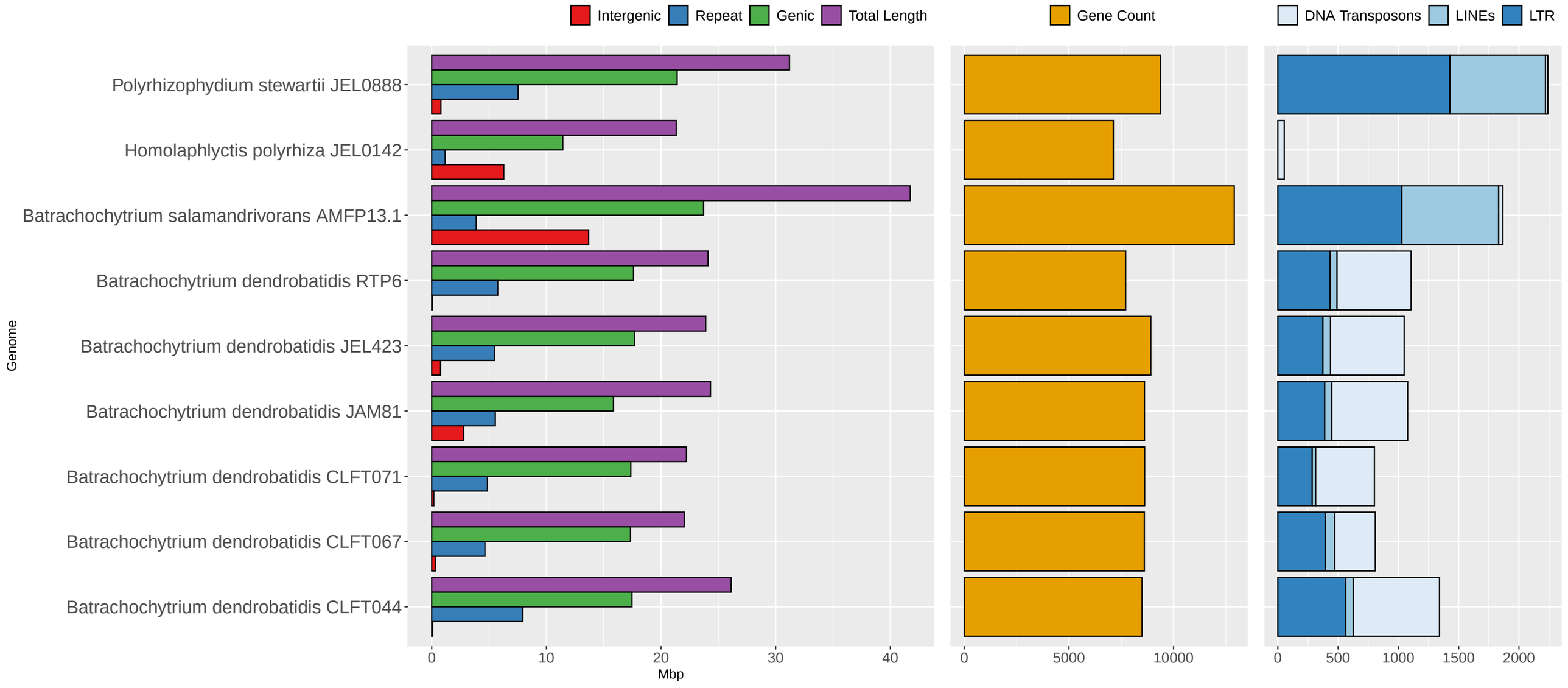
Intergenic
Repeat
Genic
Total Length
Gene Count
DNA Transposons
LINEs
LTR
Genome
Polyrhizophydium stewartii JEL0888
Homolaphlyctis polyrhiza JEL0142
Batrachochytrium salamandrivorans AMFP13.1
Batrachochytrium dendrobatidis RTP6
Batrachochytrium dendrobatidis JEL423
Batrachochytrium dendrobatidis JAM81
Batrachochytrium dendrobatidis CLFT071
Batrachochytrium dendrobatidis CLFT067
Batrachochytrium dendrobatidis CLFT044
0
10
20
30
40
Mbp
0
5000
10000
0
500
1000
1500
2000

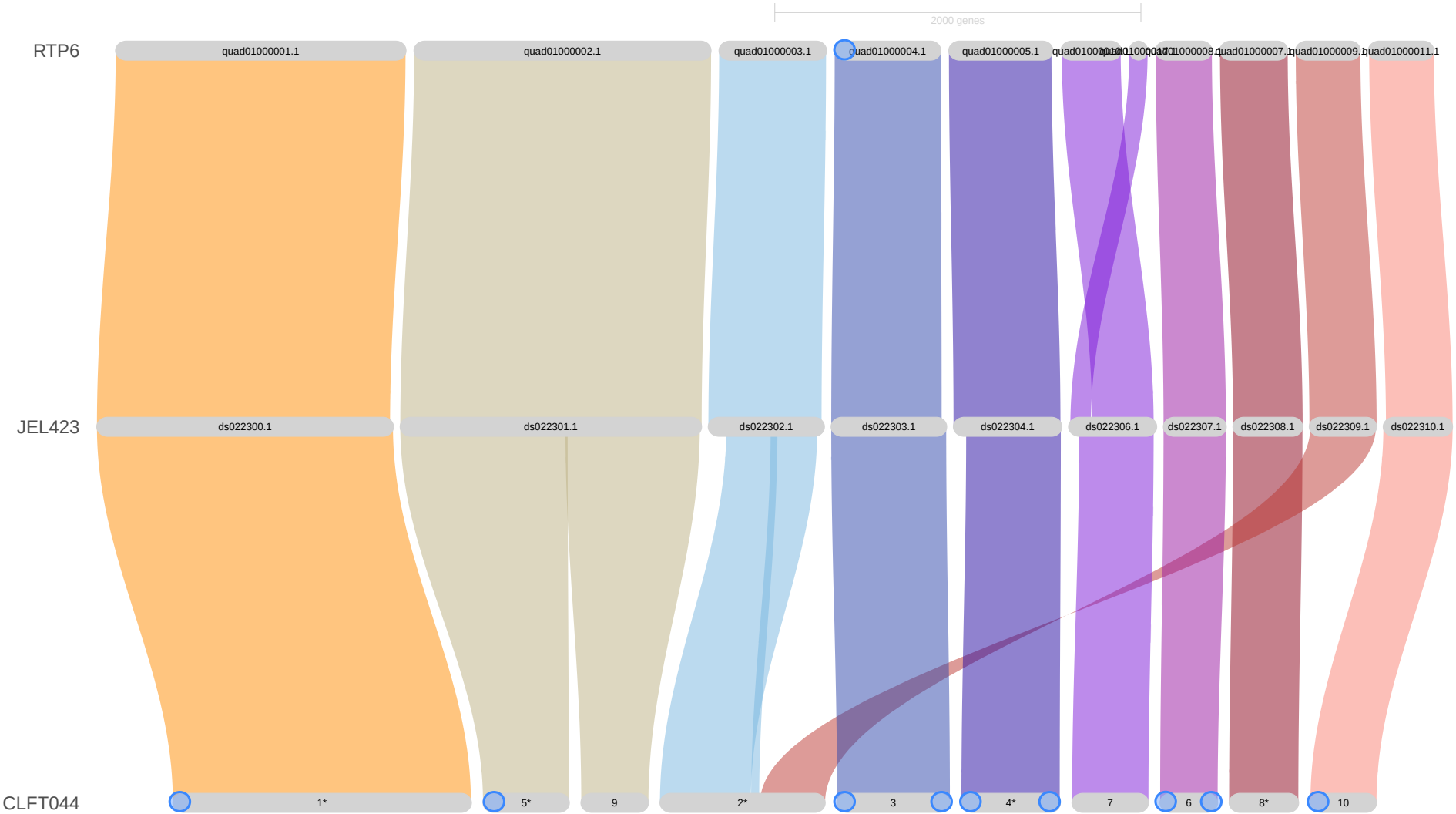

Chromosomes scaled by gene rank order

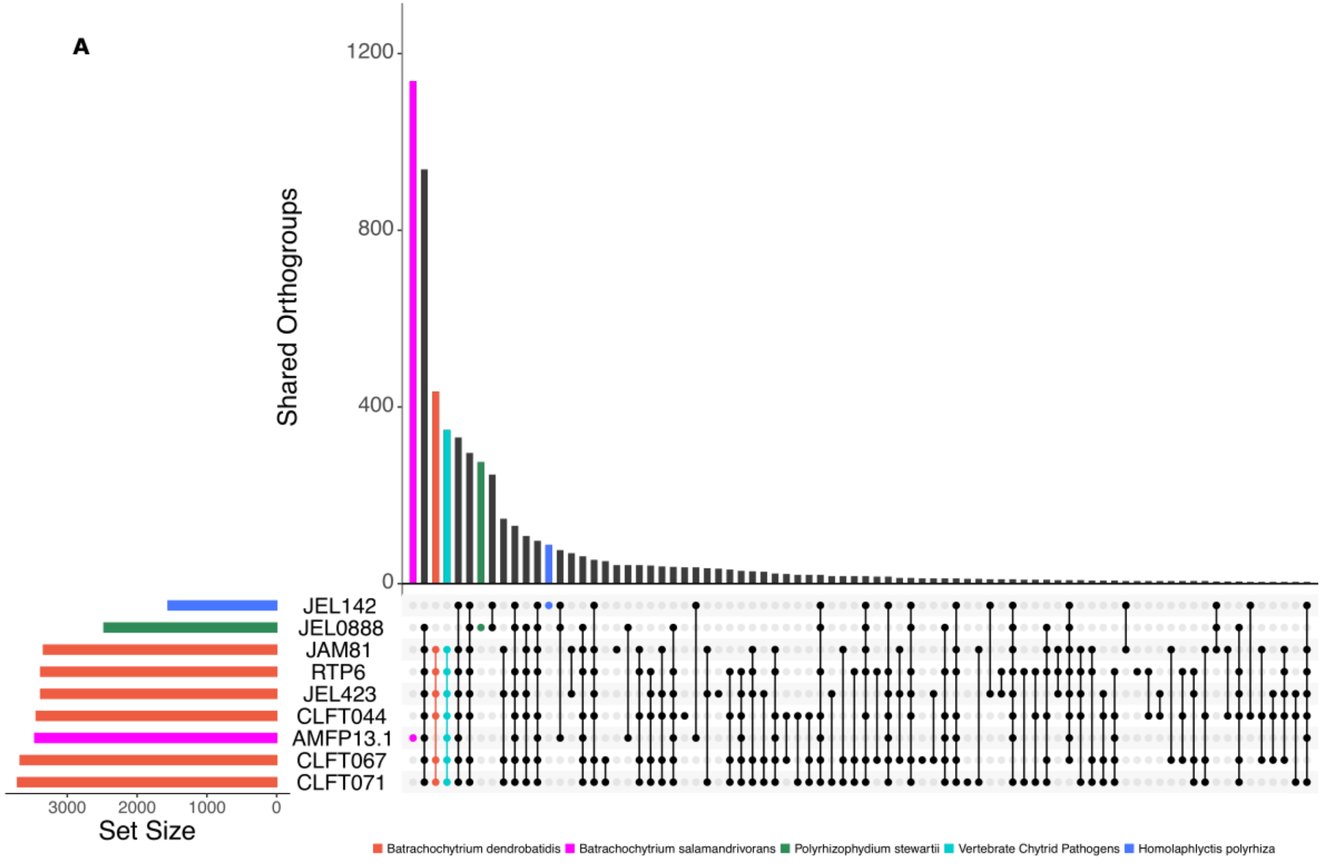
A
Shared Orthogroups
1200
800
400
0
JEL142
JEL0888
JAM81
RTP6
JEL423
CLFT044
AMFP13.1
CLFT067
CLFT071
3000
2000
1000
0
Set Size
Batrachochytrium dendrobatidis
Batrachochytrium salamandrivorans
Polyrhizophydium stewartii
Vertebrate Chytrid Pathogens
Homolaphlyctis polyrhiza

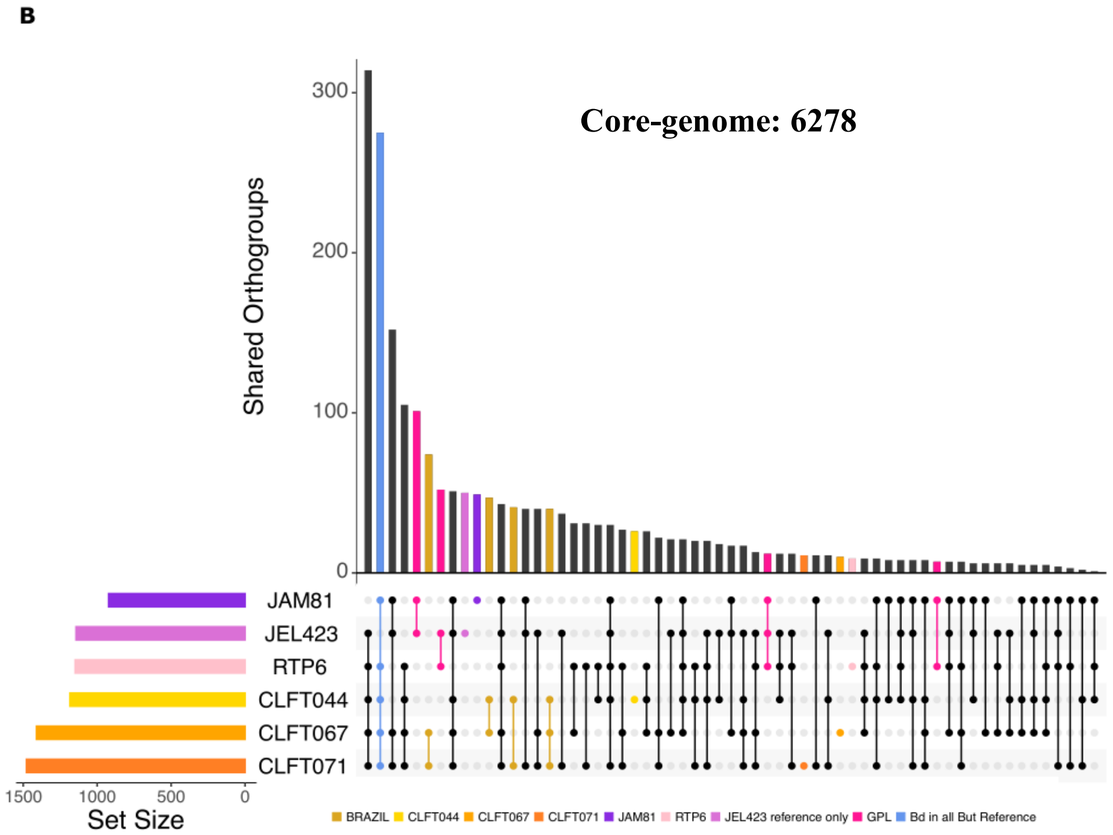
B
Core-genome: 6278
Shared Orthogroups
300
200
100
0
JAM81
JEL423
RTP6
CLFT044
CLFT067
CLFT071
1500
1000
500
0
Set Size
BRAZIL
CLFT044
CLFT067
CLFT071
JAM81
RTP6
JEL423 reference only
GPL
Bd in all But Reference

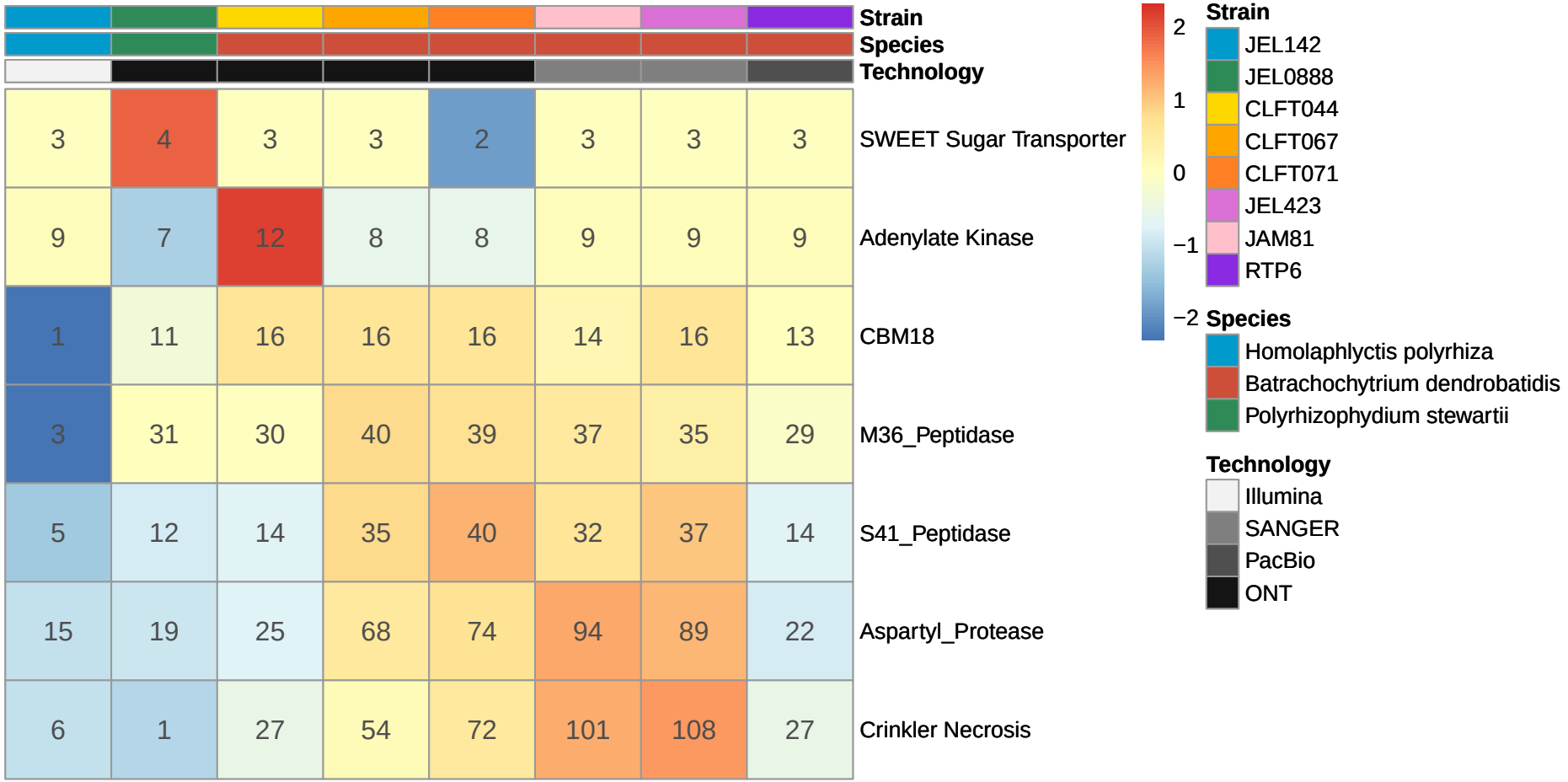
Strain
Species
Technology
3 4 3 3 2 3 3 3 SWEET Sugar Transporter
9 7 12 8 8 9 9 9 Adenylate Kinase
1 11 16 16 16 14 16 13 CBM18
3 31 30 40 39 37 35 29 M36_Peptidase
5 12 14 35 40 32 37 14 S41_Peptidase
15 19 25 68 74 94 89 22 Aspartyl_Protease
6 1 27 54 72 101 108 27 Crinkler Necrosis
2
1
0
−1
−2
Strain
JEL142
JEL0888
CLFT044
CLFT067
CLFT071
JEL423
JAM81
RTP6
Species
Homolaphlyctis polyrhiza
Batrachochytrium dendrobatidis
Polyrhizophydium stewartii
Technology
Illumina
SANGER
PacBio
ONT

A

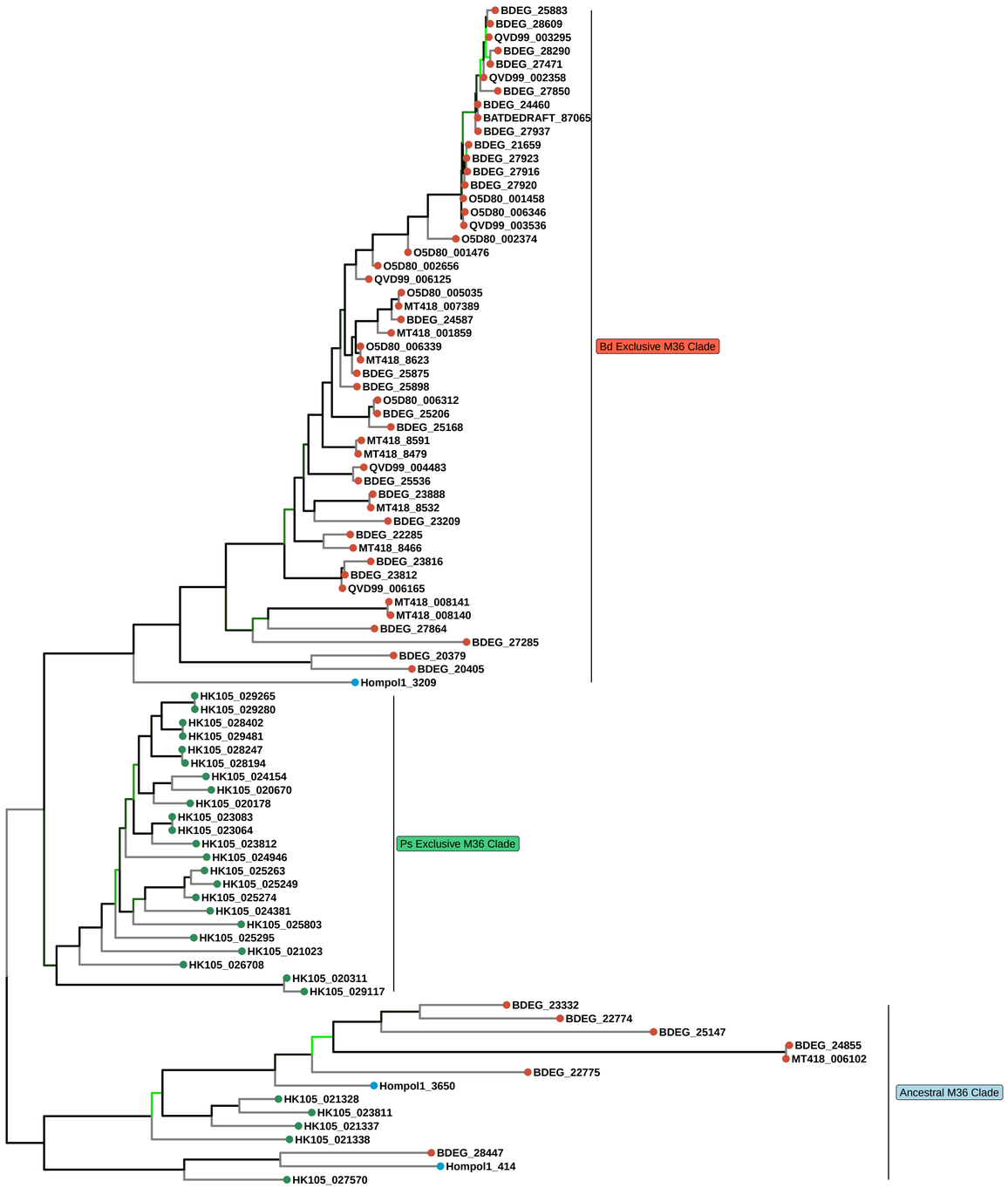

B

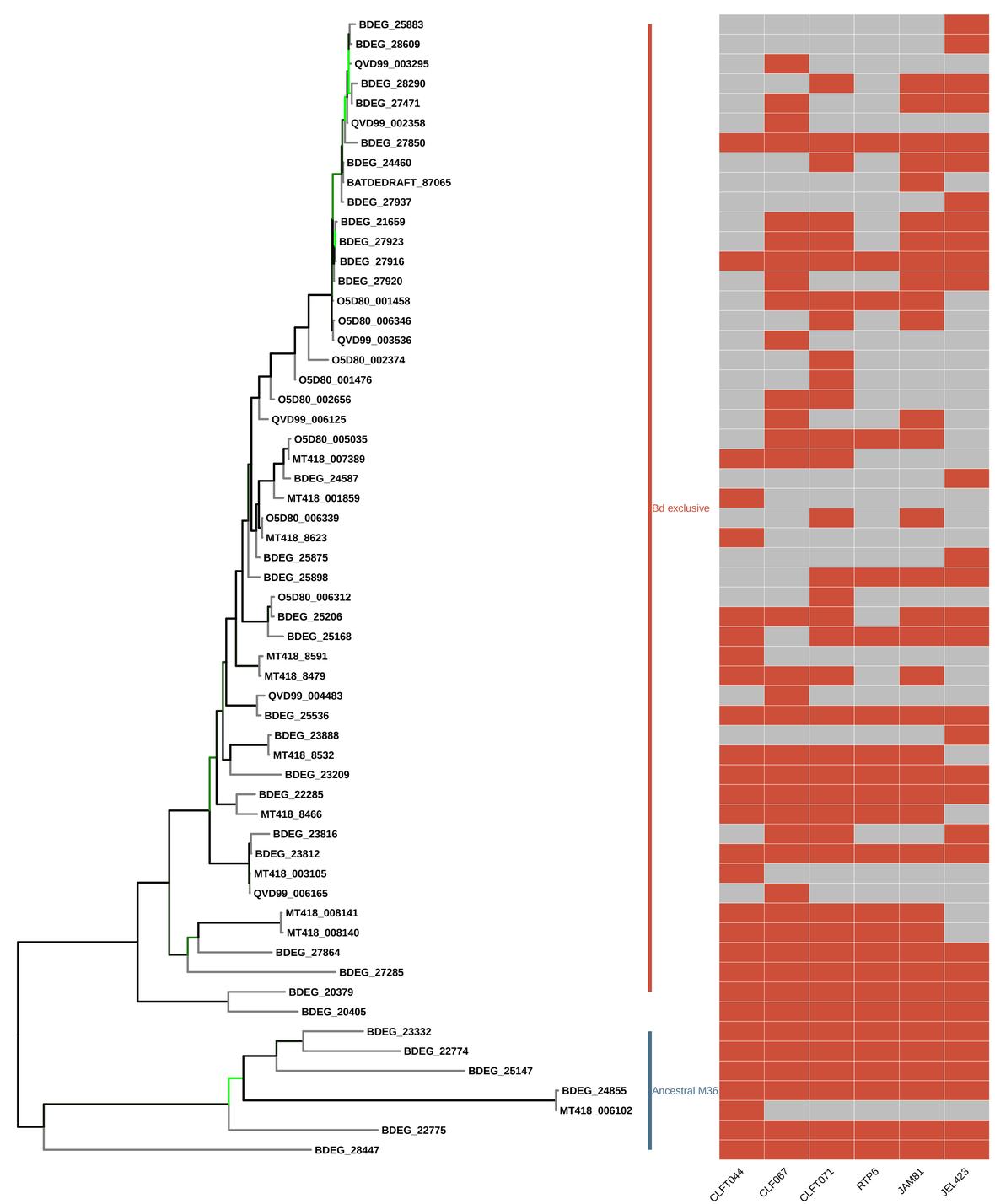

Species ● Batrachochytrium dendrobatidis ● Homolaphlyctis polyrhiza ● Polyrhizophydium stewartii

Bootstrap 0 25 50 75 100

Presence Absence Absent Present

Bootstrap 0 25 50 75 100

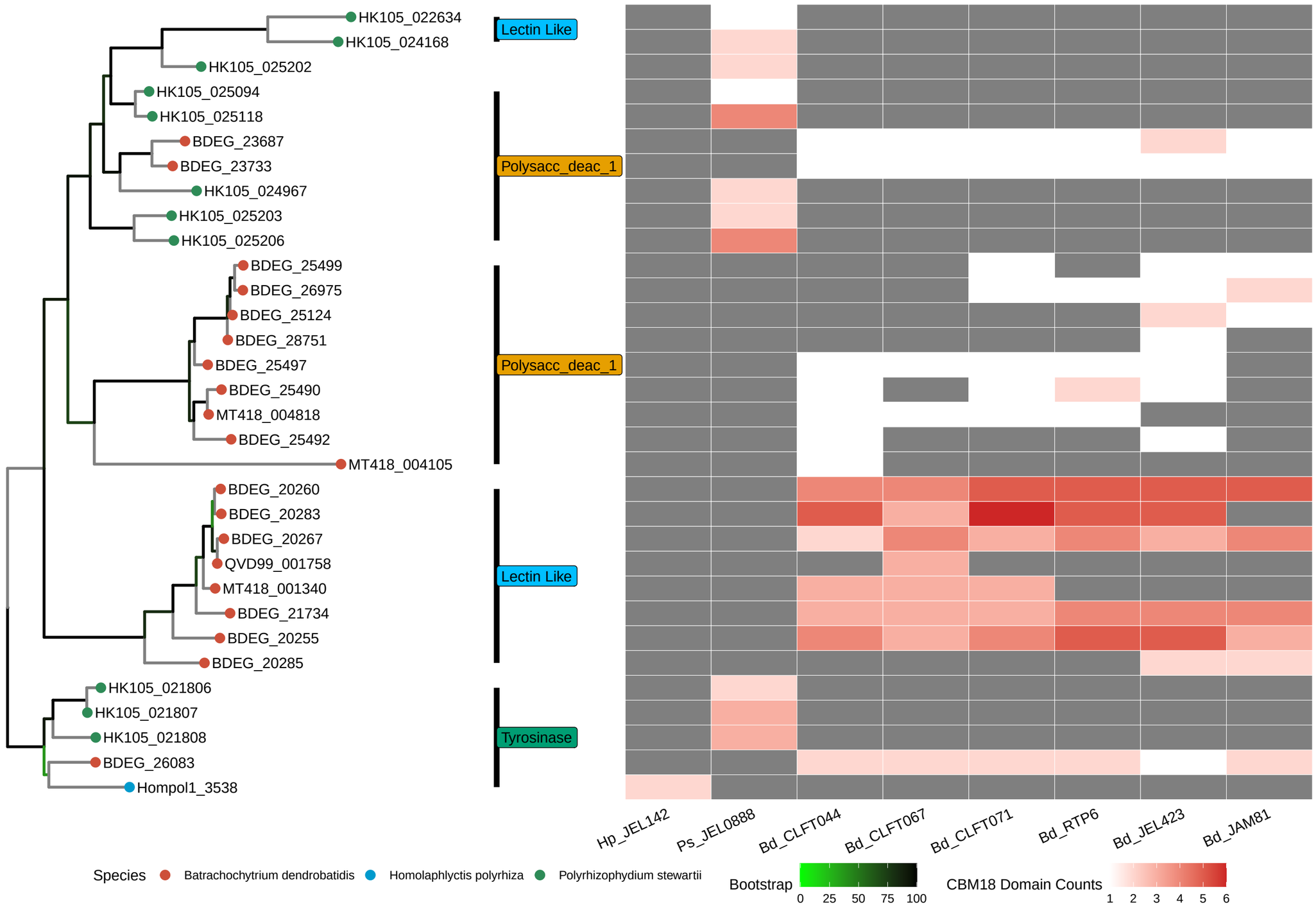
HK105_022634
HK105_024168
HK105_025202
HK105_025094
HK105_025118
BDEG_23687
BDEG_23733
HK105_024967
HK105_025203
HK105_025206
BDEG_25499
BDEG_26975
BDEG_25124
BDEG_28751
BDEG_25497
BDEG_25490
MT418_004818
BDEG_25492
MT418_004105
BDEG_20260
BDEG_20283
BDEG_20267
QVD99_001758
MT418_001340
BDEG_21734
BDEG_20255
BDEG_20285
HK105_021806
HK105_021807
HK105_021808
BDEG_26083
Hompol1_3538
Lectin Like
Polysacc_deac_1
Polysacc_deac_1
Lectin Like
Tyrosinase
Hp_JEL142
Ps_JEL0888
Bd_CLFT044
Bd_CLFT067
Bd_CLFT071
Bd_RTP6
Bd_JEL423
Bd_JAM81
Species
Batrachochytrium dendrobatidis
Homolaphlyctis polyrhiza
Polyrhizophydium stewartii
Bootstrap
0 25 50 75 100
CBM18 Domain Counts
1 2 3 4 5 6

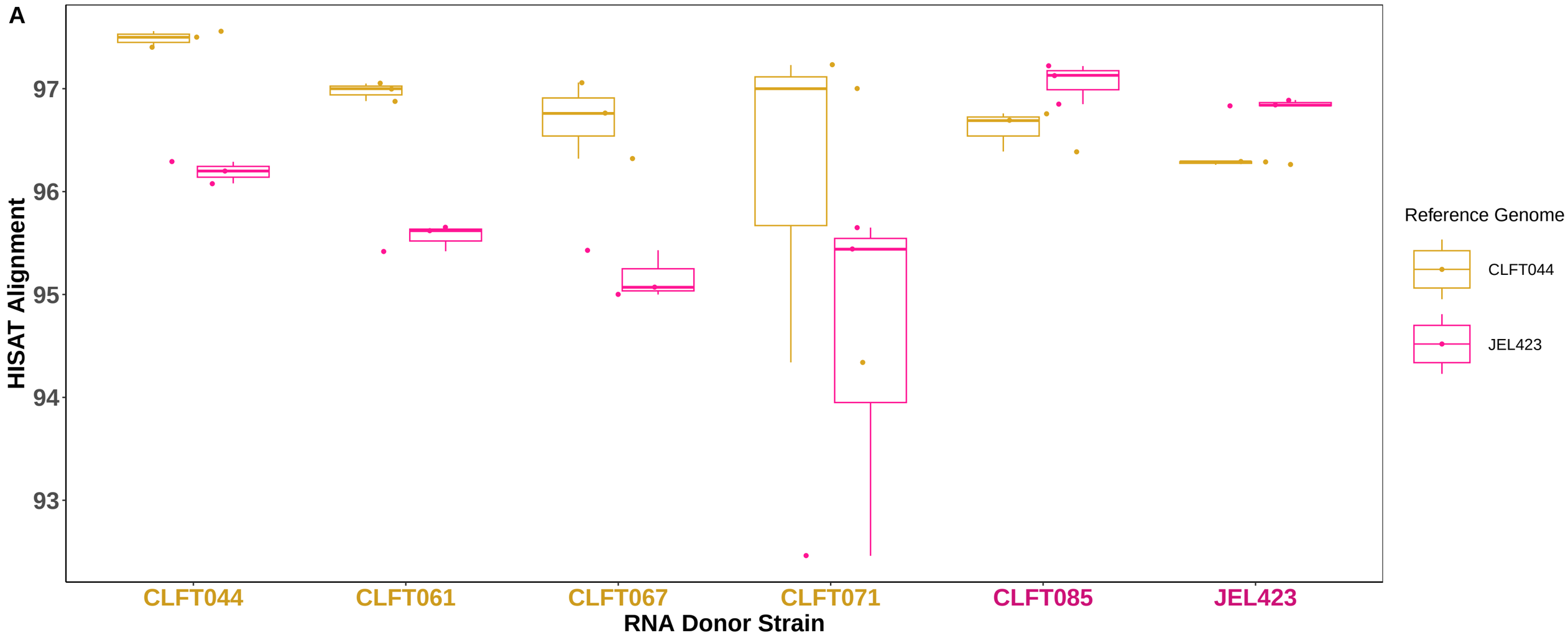
A
HISAT Alignment
97
96
95
94
93
CLFT044
CLFT061
CLFT067
CLFT071
CLFT085
JEL423
RNA Donor Strain
Reference Genome
CLFT044
JEL423

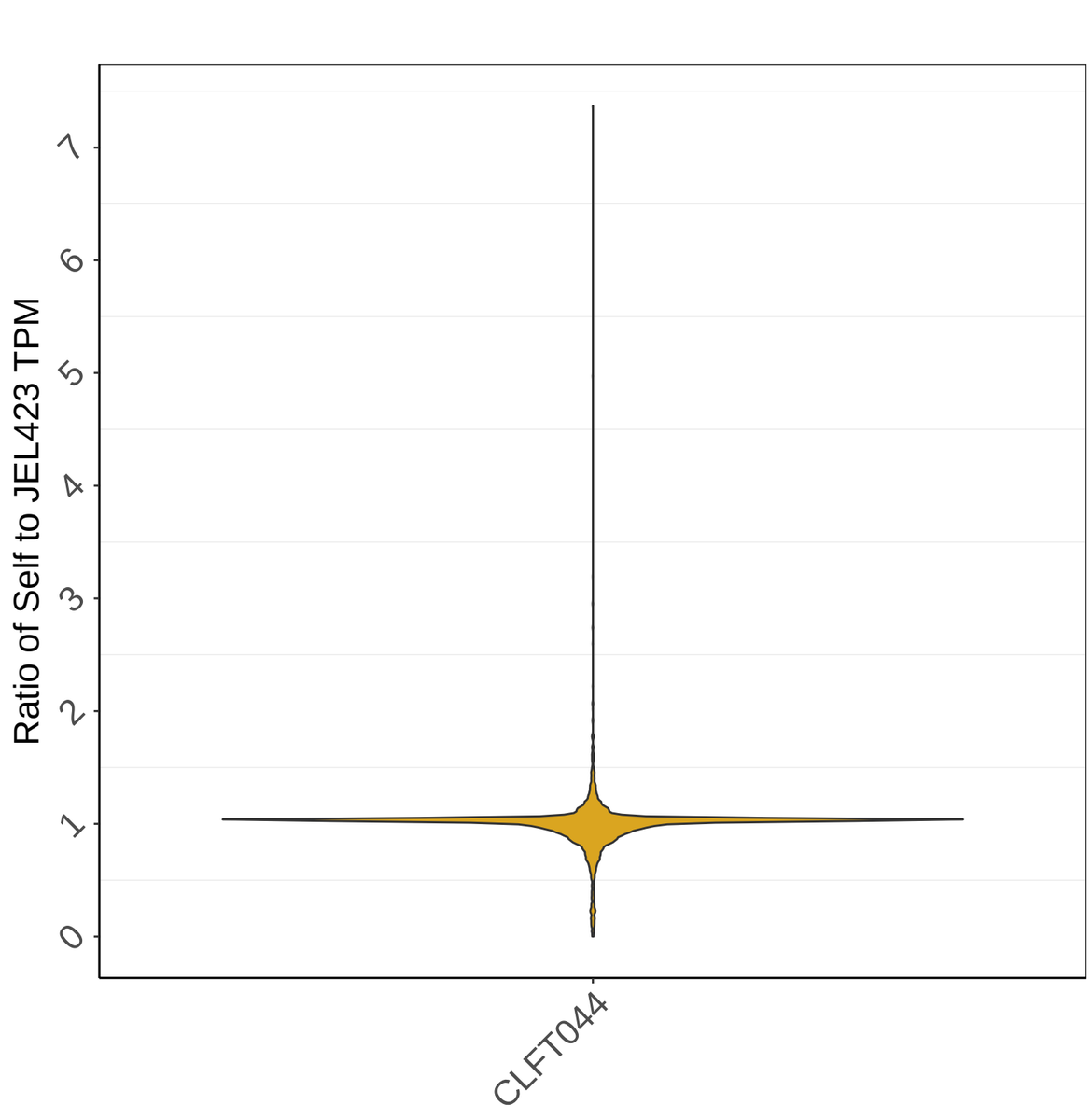
B
Ratio of Self to JEL423 TPM
0
1
2
3
4
5
6
7
CLFT044

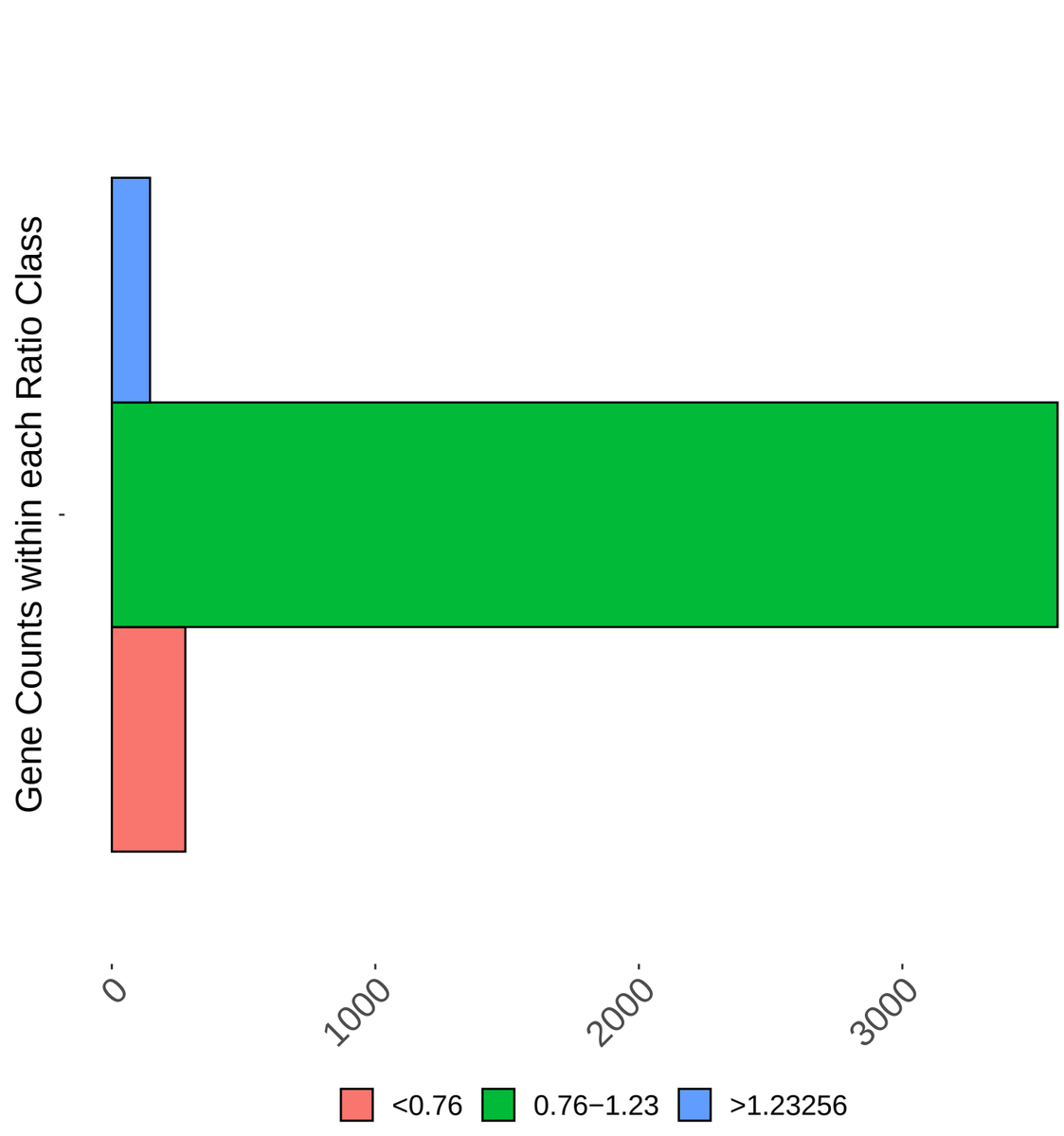
C
Gene Counts within each Ratio Class
0
1000
2000
3000
<0.76
0.76−1.23
>1.23256